Random Telegraph Signal in CMOS Image Sensor Pixels

Xinyang Wang, Padmakumar R. Rao, Adri Mierop*, Albert J.P. Theuwissen
Delft University of Technology, Delft, The Netherlands
*DALSA B.V., Eindhoven, The Netherlands

Abstract

In this work, the 1/f noise of the Source Follower (SF) in pinned-photodiode CMOS pixels is characterized. It is found that the 1/f noise in these pixels is actually due to a very limited number of traps and results in a Random Telegraph Signal (RTS). It is pointed out how the correlated-double sampling (CDS) reacts on this RTS. The temperature dependency of the imager read noise revealed two mechanisms of RTS during CDS.

Introduction

Compared to CCDs, CMOS imager sensors (CIS) suffer from high 1/f noise. Recent research (1) proved that the 1/f noise induced by traps located at the silicon silicon-oxide interface in the SF gate region becomes dominant on the pixel read noise floor in CMOS imagers. From our experiments, we found that instead of the well-known 1/f noise, it is actually a kind of "Lorentzian noise" that is exhibited, and can also be characterized as random telegraph signal (2). The pixel output depends on whether the 1/f-causing trap is filled or empty during the CDS samplings, i.e. the Probability of Trap Occupancy (PTO). The overall pixel random noise reaches a maximum if the PTOs during the two CDS samples are equal. The temperature dependency of the imager read noise revealed two mechanisms of RTS during CDS: a thermal activation mechanism and a carrier exchange mechanism. The pixel read noise reaches a maximum for temperatures at which the thermal activation dominates.

Pixel Random Noise Characterization

Fig. 1 is the circuit and readout timing diagram of a 4T CIS pixel, as used in our experiments. During the pixel readout period, the reset transistor (RST) is off. The RS and the S/HR are enabled first to sample the reset voltage of the floating diffusion. After the charge transfer, the RS and the S/HS are enabled to sample the video signal. By subtracting these two samples, the correlated transistor offset and thermal noise from the reset transistor are cancelled.

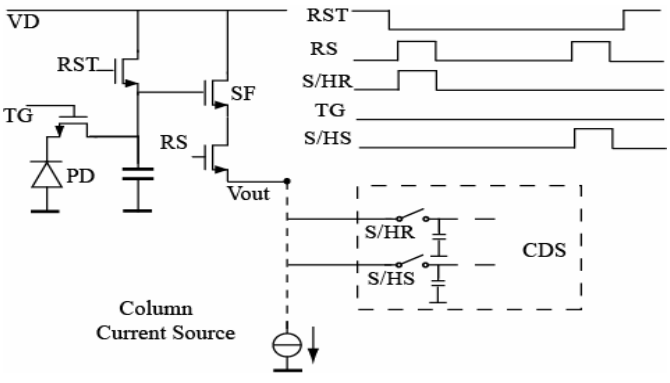

Figure 1: Circuit and readout timing diagram of 4T CIS pixel, transmission gate (TG), reset transistor (RST), source follower (SF), row selector (RS), photodiode (PD) and hold/sample of CDS (S/HR and S/HS)

For the measurements, the TG is grounded as shown in Fig.1 to minimize the dark current random noise from the photodiode. The dark random noise histogram of all pixels is shown in Fig. 2. The random noise of each pixel is obtained by calculating the standard deviation of 20 frames' outputs. The asymmetric distribution of the pixels around the peak indicates the dominating 1/f noise of the SF (3). It is shown that the 1/f noise of the SF becomes dominant on the pixel read noise floor. Apparently, the 1/f noise is not fully correlated in the samples of CDS, therefore can not be eliminated completely.

To further investigate the characteristics of the dominating 1/f noise, the noise histogram in Fig.2 is divided into different parts. Fig. 3 plots the temporal output behavior of pixels belonging to each parts of the noise histogram. Each plot is made up from 1500 frames in order to have enough samples to show the different noise characteristics. As can be seen in Fig.3, for most of the "quiet" pixels, e.g. pixel A and B, the output is fairly constant. The random noise of these pixels is normally below 20 Digital Number (DN), and is dominated by the thermal noise. However, three discrete levels can already be seen from the temporal output of pixel C. Because the frequency of the appearance of the highest and lowest discrete levels is small, the overall pixel noise is small.

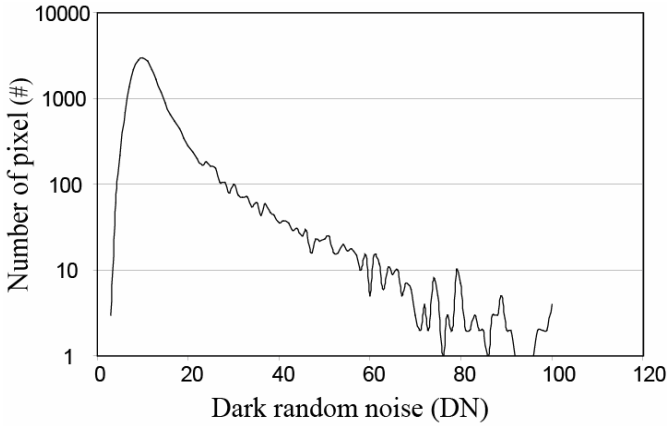

Figure 2: Dark random noise histogram of pixels (in digital numbers)

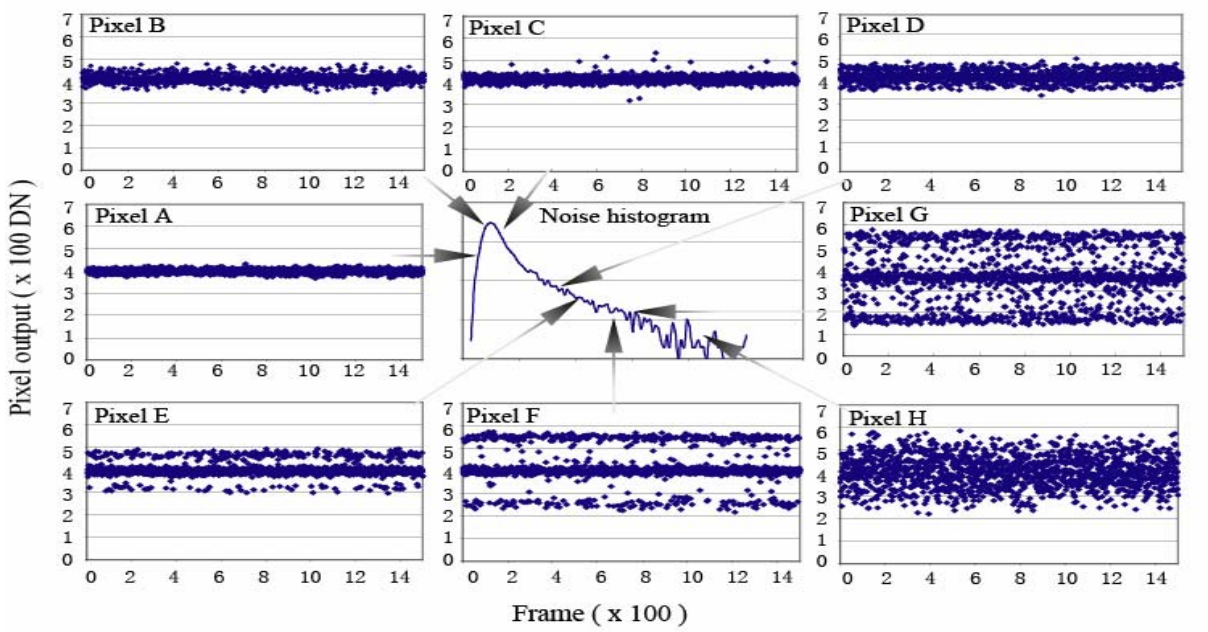

Figure 3: Temporal output behavior of pixels belonging to different parts of the noise histogram of Fig.2

Among all the "noisy" pixels, the majority exhibit similar discrete levels, as shown by pixel D, E, F and G. The frequencies and the amplitudes of the upper/lower levels determine the pixel read noise. Pixel H is one of the noisiest pixels, and the discrete levels are no longer visible.

Fig. 4 explains the origin of the discrete levels of the pixel temporal outputs. For the pixel in which the SF contains only one active trap in or near the channel interface, it is possible to observe two discrete output levels because of the trapping and releasing of the minority carriers (4). The trapped minority carrier changes the amount of conductive carriers and also influences the channel surface potential, both of which influence carrier mobility. The RTS effect is particularly pronounced in the case of a small conductive current. Consequently, the CDS produces three discrete levels as shown. The lower level is generated if a falling edge of RTS occurs between two samples. The higher level is generated in the case of a rising edge. If both samples are in the same RTS status, the CDS output falls into the middle level.

PTO Measurement and Characterization

To study how the RTS is determined by the trap properties, we introduce the concept of PTO, Probability of Trap Occupancy. Fig. 5 is the histogram obtained from Fig.4. It is pointed out how the pixel output level is determined by P_1 during the first sample (see insert in Fig.5) and P_2 during the second sample (see insert in Fig.5). The probability of the

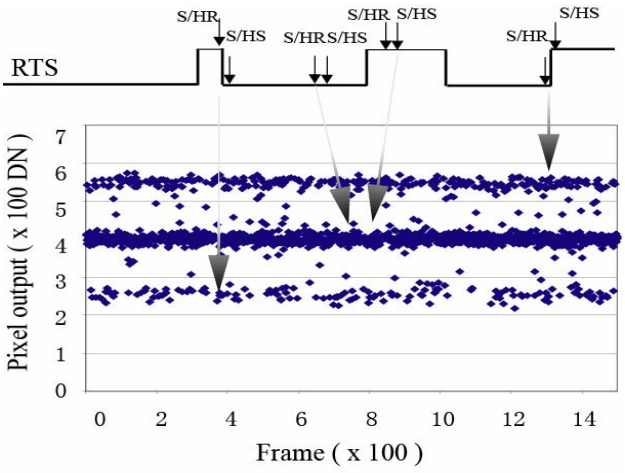

Figure 4: Correlated double sampling of RTS

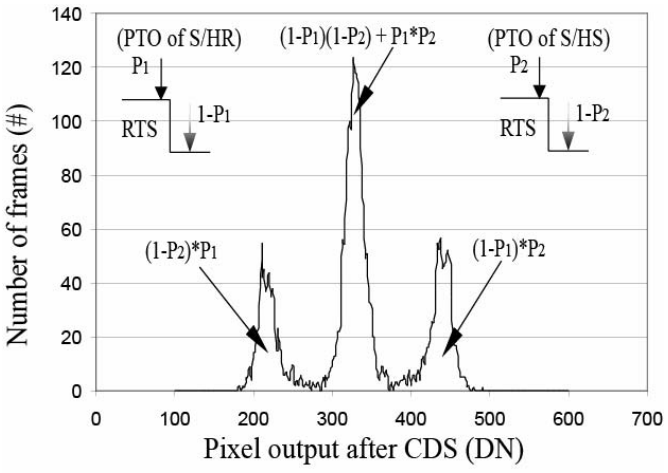

Figure 5: Temporal output histogram, P_x is the PTO during samplings

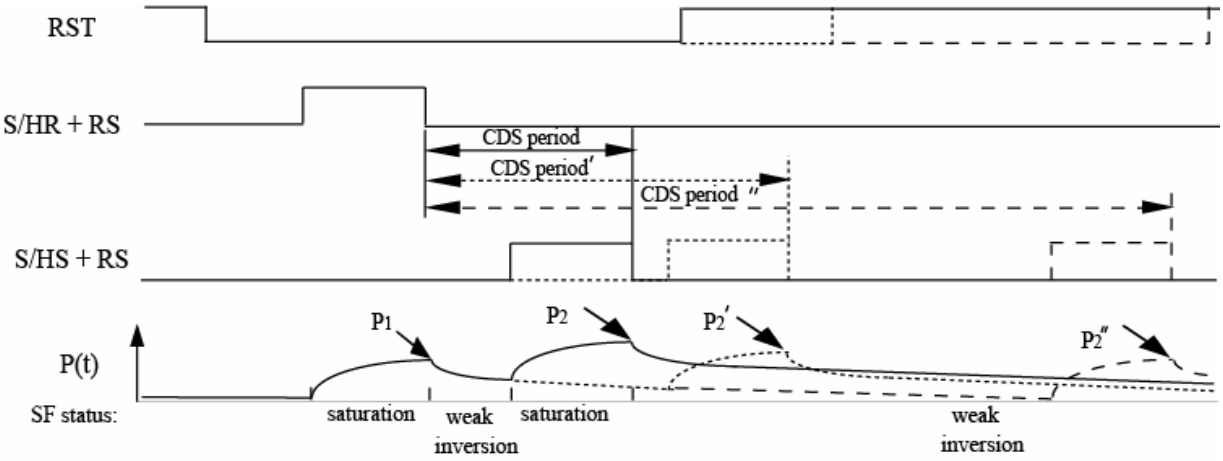

Figure 6.The readout timing diagram, the SF status and the transient PTO (P(t)). The SF operates in saturation during each sample and in weak inversion because of the disconnecting with the column current source between two sample periods.

pixel output being located in the lower peak is $(1-P_2)*P_1$. Similar equations can be written for the higher and the middle peaks. Therefore, the PTO can be calculated through the histogram shown in Fig.5.

Fig.6 shows the timing diagram, the SF status and the transient PTO during pixel read out. To avoid the read destruction from the sampling capacitor and the column discharge, the RS is only enabled during the S/H pulse as shown in Fig.6. Therefore, the SF transistor switches between weak inversion and saturation during the CDS. The transient PTO value shown in Fig.6 is determined by the trap capture time (τ_c) and emission time (τ_e) (5, 6) where:

$$P(t) = \frac{\tau_e}{\tau_c + \tau_e} + K \cdot \exp\left[-\left(\frac{1}{\tau_e} + \frac{1}{\tau_c}\right)t\right]$$

and where K is the integration constant and where t is the time (2). As shown, with increasing the CDS period, P_1 does not change while P_2 attenuates because of the reduction of its initial value. To confirm the analysis in Fig.6, the PTO values are calculated from the measurement data. Fig. 7 plots the calculated PTO values with different CDS clock periods. The P_1 and P_2 dependencies fully agree with the previous analysis. It is seen that P_2 reduces with an increasing CDS period, while P_1 is independent of the CDS period. If the CDS period is long enough, then from the analysis of Fig.6, the PTO during the first and the second sample starts at the same value, and with equal CDS pulses, P_2 equals P_1. In our experiment, it is shown that when P_1 equals P_2, the "side peaks" of the histogram are identical and the symmetric histogram at this moment yields maximum pixel read noise.

Fig. 8 shows the measured PTO dependency on temperature. It can be seen that there is a turning point temperature for both P_1 and P_2. The highest left/right peaks in the histogram at this temperature give the maximum pixel read noise. Fig. 9 explains two mechanisms causing this turning point. In

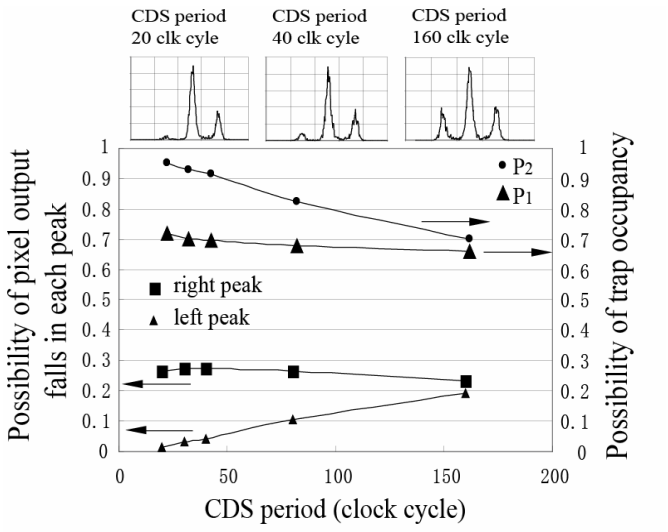

Figure 7: Calculated PTO dependency on CDS period from the measurement

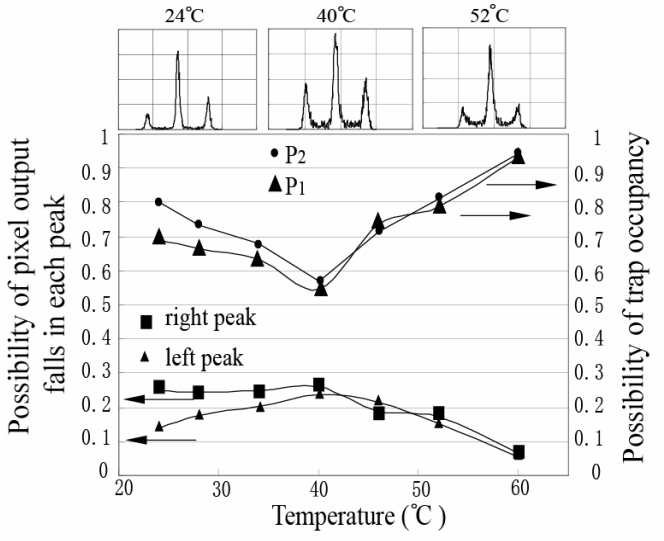

Figure 8: Calculated PTO dependency on temperature from the measurement

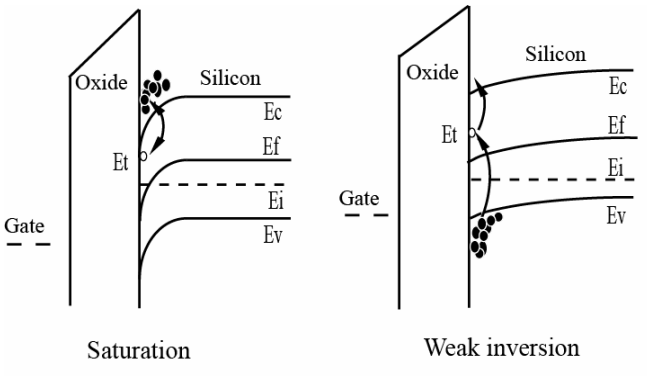

Figure 9: RTS mechanisms during CDS

saturation, the current fluctuation is mainly due to the exchange of carriers between the conduction band and the trap. Both τ_e and τ_c decrease with increasing the temperature. The overall PTO decreases since τ_e reduces faster (5). This effect dominates at the temperature below the turn-point and is also observed in (7). In weak inversion, the trapped carrier is thermally activated mainly from the valence band. Increasing the temperature makes the activation easier and therefore PTO increases, which dominates after the turn-point.

Infrared light illumination is used in the experiment to verify this model. Illuminating the sample with infrared photons has the same effect as increasing the temperature for the thermal activation mechanism, but has little effect on the carriers exchange mechanism. Fig. 10 plots the theoretical and measured P_1 and P_2 dependencies on illumination with infrared light. In saturation, the RTS effect is mainly due to the carrier exchange mechanism, therefore, the PTO is independent of illumination. In weak inversion, the infrared photons supply energy to the electrons in the valence band and therefore increase the PTO.

Conclusion

For the first time, RTS is observed and studied in pinned-photodiode CMOS image sensor pixels. For imagers made in a 0.18μm CMOS process, the actual dominating pixel read noise is discrete and dominated by a single interface trap in the SF. The CDS influence on RTS noise highly depends on the CDS period and the trap properties. The overall pixel random noise reaches a maximum if the PTOs during the two CDS samples are equal. The temperature dependency of the imager read noise revealed two mechanisms of RTS during

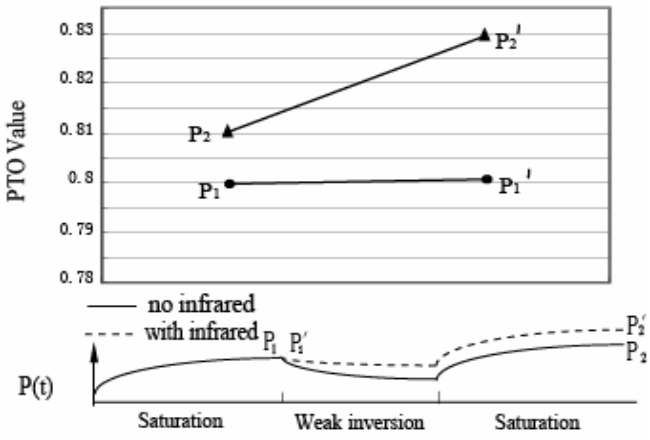

Figure 10: Theoretical and measured PTO dependency on infrared light

CDS: a thermal activation and a carrier exchange mechanism. At the temperature where the thermal activation mechanism becomes dominant, the pixel shows the highest value of read noise.

Acknowledgement

The authors would like to thank their colleague M.F.Snoeij from TU Delft for helpful technical discussion and Daniel Verbugt, Willem Hoekstra, and Willy Maes from DALSA BV for supplying the test structure and the simulation data.

References:

(1) J.Y.Kim, et.al. "Characterization and improvement of random noise in 1/3.2" UXGA CMOS image sensor with 2.8um pixel using 0.13um-technology," *IEEE Workshop on CCDs & AIS. Japan,* pp.149-152, June 2005

(2) A.P.van der Wel, "MOSFET LF noise under large signal excitation: measurement, modeling and application," PhD Thesis, 2005

(3) B.Pain, T.Cunningham, B.Hancock, C.Wrigley, and C.Sun, "Excess noise and dark current mechanisms in CMOS imagers," *IEEE Workshop on CCDs & AIS. Japan*, pp.153-156, June 2005

(4) G.I.Wirth, J.Koh, R.Silva, R.Thewes, and R.Brederlow, "Modeling of statistical low-frequency noise of deep-submicrometer MOSFETs," *IEEE Trans. on Electron Devices*, pp1576-1588, July 2005.

(5) K.K.Hung, P.K.Ko, and C.Hu, "Random telegraph noise of deep-submicrometer MOEFET's," *IEEE Electron Device Letters,* Vol.11, pp 90-92, Feb 1990

(6) A.P.van der Wel, E.A.M.Klumperink, L.K.J.Vandamme, and B.Nauta, "Modeling random telegraph noise under switched bias conditions using cyclostationary RTS noise," *IEEE Trans on Electron Devices*, pp1378-1384, May 2003

(7) J.Janesick, J.Andrews, and T.Elliott, "Fundamental performance differences between CMOS and CCD imagers," in press.